nature structural & molecular biology

Direct observation of the myosin-Va power stroke and its reversal

James R Sellers[1] & Claudia Veigel[2,3]

Complex forms of cellular motility, including cell division, organelle trafficking or signal amplification in the auditory system, require strong coordination of the myosin motors involved. The most basic mechanism of coordination is via direct mechanical interactions of individual motor heads leading to modification of their mechanochemical cycles. Here we used an optical trap–based assay to investigate the reversibility of the force-generating conformational change (power stroke) of single myosin-Va motor heads. By applying load to the head shortly after binding to actin, we found that, at a certain load, the power stroke could be reversed, and the head fluctuated between an actin-bound pre– and a post–power stroke conformation. This load-dependent mechanical instability might be critical to coordinate the heads of processive, dimeric myosin-Va. Nonlinear response to load leading to coordination or oscillations amongst motors might be relevant for many cellular functions.

Class Va myosins are ATP-driven two-headed motor proteins expressed in neurons and melanocytes that transport neuronal vesicles and melanosomes along actin[1]. The motor moves its cargo processively, taking tens of 36-nm steps per interaction event[2–5]. Each myosin head consists of an N-terminal catalytic domain that hydrolyzes ATP and binds actin. This is followed by the neck domain, an extended α-helix, stabilized by binding light chains of the calmodulin family, that serves as a lever arm. The neck extends into a coiled-coil dimerization and cargo-binding domain. It is generally thought that, during each biochemical cycle, a single myosin-Va motor head binds to actin with hydrolysis products phosphate and ADP bound. According to the power-stroke model, actin binding induces phosphate release and a force-generating conformational change of the bound head. This leads into an ADP-bound state. When ADP is released, a second, smaller conformational change takes place before the head finally binds a new ATP, detaches from actin and hydrolyzes the ATP[3,4,6–8]. Evidence for an actin-bound pre–power stroke state (pre-state) preceding the main conformational change comes from crystal structures of myosin alone[9] and electron micrographs of myosin-Va bound with both heads to actin[10,11]. In the latter studies, backward- and forward-leaning orientations of the base of the lever arm could be distinguished that are thought to correspond to pre– and post–power stroke conformations (post-state). The model motivated by these data postulates that each processive step of dimeric myosin-Va along actin causes the neck domains of the two bound heads to switch orientation in a reciprocal manner: the leading head switches from the backward- to the forward-leaning orientation and the trailing head from the forward- to the backward-leaning orientation. These orientations have then been studied by attaching fluorescent labels to the neck domains[12,13]. In a number of pioneering experiments, translational[14–16] and rotational motion of the neck (using microtubule fragments as markers of angular motion)[17] during transitions between successive, actin-bound orientations were also resolved. However, the reversibility of the transition from pre- to post-state has never been directly observed. It has been shown that dimeric myosin-Va stalls at a load of ~2 pN[2,4,16,18] and slides backwards at higher forces[19], similarly to kinesin-1(ref. 20). It had remained unclear, however, whether these backward movements involve power-stroke reversal or whether the molecule simply unbinds and rebinds. An interesting regulatory mechanism would emerge if the power stroke could be reversed while the motor stayed attached to actin. This would cause a sudden release of tension under load (that is, a negative compliance) without cargo detachment. We therefore set out to test the reversibility of the power stroke of a single myosin motor head using single-molecule mechanical experiments.

RESULTS

Detection of power-stroke reversals

To investigate whether the force-generating conformational change of a single myosin head is reversible and whether we could resolve transitions between pre- and post-state, we designed an optical trap–based single-molecule experiment with which we could rapidly detect myosin binding and subsequently apply constant backward load. We used a three-bead assay where we immobilized recombinant, single-headed myosin-Va constructs containing six IQ motifs (hereafter called MVS1)[21] on surface-attached beads and allowed them to interact with an actin filament suspended between two beads held in optical traps[22,23] (**Fig. 1a**). We used a high ATP concentration (100 μM) to approximate physiological conditions and to make sure that the nucleotide-free rigor state was short-lived (see below). We determined the force acting on the actin filament by the displacement Δx of the

[1]Laboratory of Molecular Physiology, National Heart, Lung, and Blood Institute, National Institutes of Health, Bethesda, Maryland USA. [2]Physical Biochemistry, National Institute for Medical Research, London, UK. [3]Department of Cellular Physiology, Ludwig Maximilians University Munich, Munich, Germany. Correspondence should be addressed to C.V. (claudia.veigel@med.uni-muenchen.de).

Received 22 July 2009; accepted 25 February 2010; published online 25 April 2010; doi:10.1038/nsmb.1820

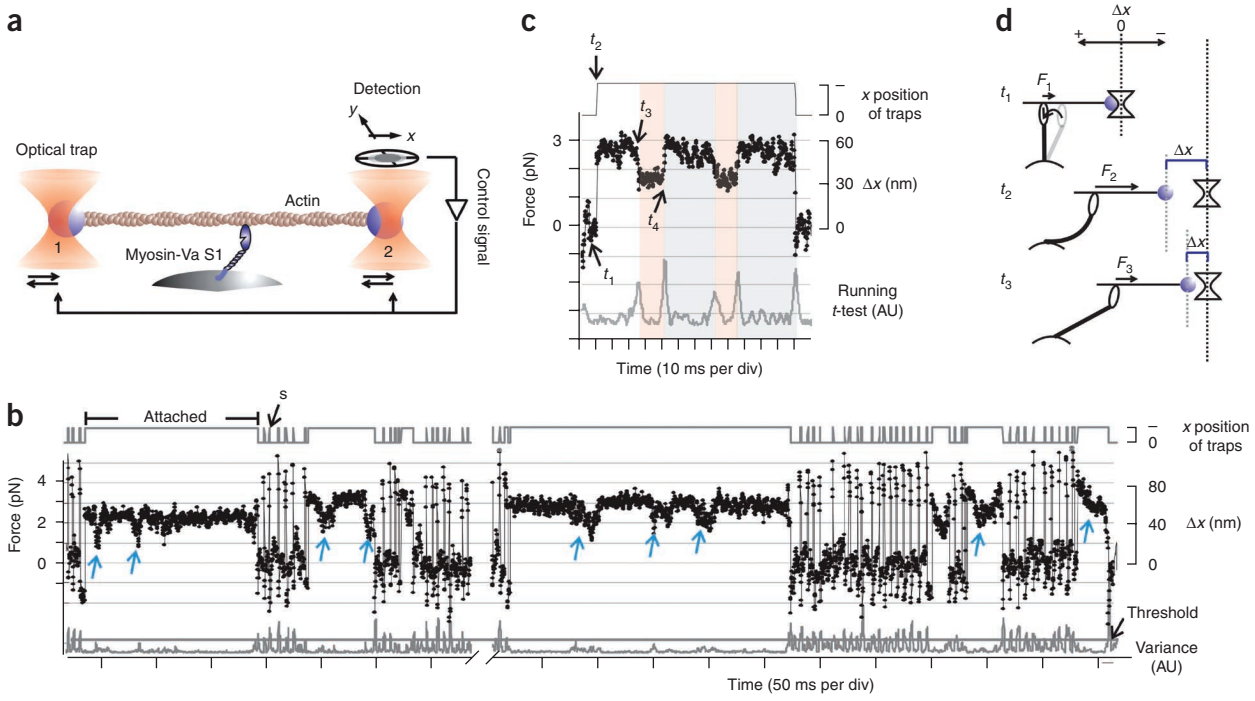

Figure 1 Single MVS1 molecules interacting with actin under load. (**a**) MVS1 on surface-attached beads interacting with F-actin suspended between two polystyrene beads held in optical traps. On-line detection of myosin binding was used to control trap position and to trigger trap displacement parallel to the actin-filament axis to apply load. (**b**) Displacements produced by bound myosin at different resisting forces (5 kHz sampling rate). Δx is bead position relative to trap position and determines force F on myosin; $F = 2\kappa_{trap}\Delta x$; κ_{trap}, single-trap stiffness. The threshold to trigger trap displacement was tuned to keep the trap positions fixed during attached periods, whereas spurious trap displacements (arrow *s*) were tolerated during unbound periods. (**c**) In a typical binding event, initial binding and conformational change in the $+\Delta x$ direction occurred around time point t_1 at <0.5 pN load and were not resolved separately. Load was applied at time t_2, and at t_3 a negative displacement (see also blue arrows in **Fig. 1b**) occurred, consistent with power-stroke reversal, followed by a positive displacement at t_4. (**d**) Cartoon shows the sequence of trap displacement and bead movement when force is applied. Significant back-and-forth displacements were detected using a running *t*-test as shown in **Figure 1b**. The experiments were carried out at 100 μM ATP.

trapped beads from the centers of the traps. To increase time resolution in detecting myosin binding, we rapidly oscillated bead 1 (1 kHz) with a small amplitude while monitoring the position of bead 2, as in earlier studies[21]. We detected the time point of myosin binding on-line by analyzing the change in amplitude of the sinusoidal forcing function transmitted from bead 1 to bead 2 (see Online Methods) and setting a threshold. Thermal noise caused false alarms in the detection of binding and detachment. By appropriately setting the threshold for detecting binding, we could shift the false alarms to either the unbound or bound state; we chose the former. To probe for power-stroke reversal, we applied backward loads varying between 2–7 pN by displacing both traps rapidly by a fixed distance immediately after detecting binding (Online Methods and **Supplementary Fig. 1a**). We tuned the threshold for detecting binding such that the position of both traps was stationary during myosin attachment events, whereas spurious trap displacements were tolerated during the unbound periods (**Fig. 1b**). We could thus follow conformational changes of the bound motor under near-constant loads with ~1-ms time resolution. As soon as we detected myosin detachment, we returned the traps to their initial positions and resumed the oscillations so that the sequence could be repeated. The power stroke following initial binding was not resolved within our time resolution of ~1 ms, and it is likely that, at low load, we only detected myosin binding after the motor had reached the post-state[23,24]. During attachment, we observed intermittent back-and-forth displacements (**Fig. 1b**, blue arrows), consistent with a reversal of the initial conformational change.

Detailed inspection of a typical binding event (**Fig. 1c**) allowed us to assign time points of transitions (cartoon, **Fig. 1d**). Myosin binding and (the unresolved first) power stroke happened around time point t_1. With an ~3-ms delay, both traps were displaced at t_2 such that a backward load of ~3 pN was applied. Note that the displacement occurring between t_1 and t_2 is due to the movement of the traps and not a power stroke. Variables and geometry are defined in **Figure 1d**. At t_3, a negative displacement ('reversal') of ~20 nm occurred, followed by a positive displacement ('recovery') of similar amplitude at t_4 (**Fig. 1c**). This shows that the bound motor could reverse into the pre-state but subsequently also recover its post-state.

Load-dependent amplitudes of reversals and recoveries

Next, we analyzed the amplitudes of the reversals and recoveries to test whether they correspond to complete power strokes (**Fig. 2**). We used a running *t*-test to detect transitions between distinct bound positions (**Fig. 1c** and Online Methods) and found transitions in ~20–30% of binding events at forces between 2–7 pN, whereas we did not observe transitions at forces below 1.5 pN (**Fig. 2a** and **Supplementary Fig. 1c**). We found up to seven back-and-forth transitions per binding event at forces between 2–3 pN, whereas above 5 pN, transitions were overwhelmingly backwards (**Fig. 2d**). The average number of transitions per binding event over the entire force range (2–7 pN) was ~1.6 (**Supplementary Fig. 1d**). The majority (60–70%) of final transitions before detachment were reversals at

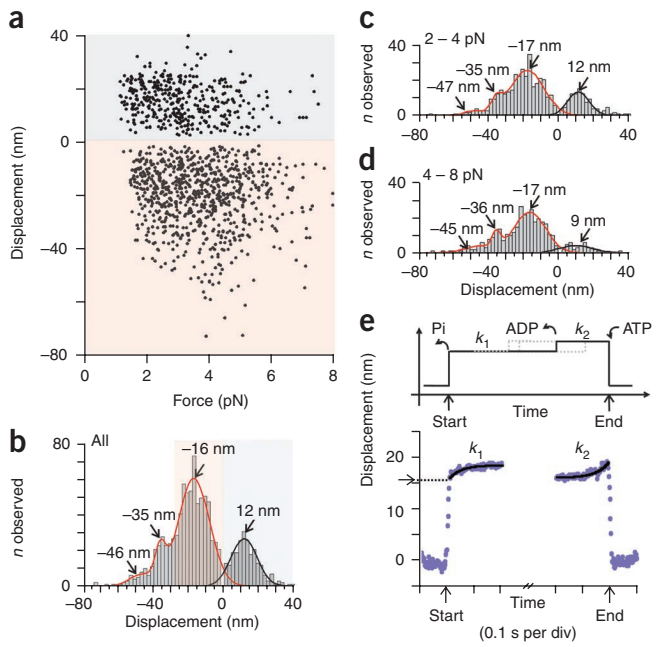

Figure 2 Statistical analysis of reversals and recoveries. Negative displacements (reversals) and positive displacements (recoveries) were detected using a running *t*-test. (**a**) Amplitudes of reversals (red) and recoveries (gray) were measured relative to the level preceding the displacement step and plotted against load. (**b**) Distributions of reversals and recoveries (n = 1,020), measured over 2–7 pN forces, were fitted by sums of Gaussians. (**c**,**d**) Subsets of reversals and recoveries were measured over 2–4 pN and 4–8 pN, respectively. (**e**) Ensemble averaging[4] of binding events (n = 225) was used to determine amplitudes and transition rates of the MVS1 two-step power stroke at low load (<2 pN) and low ATP (10 μM ATP). The model describes the two substeps of the MVS1 power stroke coupled to the release of hydrolysis products phosphate and ADP. The dashed lines indicate stochastic timing of ADP release (k_1 = 24 s^{-1}). The nucleotide-free state following ADP release is terminated by ATP binding (k_2 = 23 s^{-1}) (refs. 6,7,26).

all forces (**Fig. 1b** and **Supplementary Fig. 1e**). This suggests that the motor in the pre-state is less strongly bound[6,7,19]. To be less sensitive to slow baseline drift, we measured the amplitudes of both reversals and recoveries as relative displacements in **Figure 2a** (relative to the positions preceding the respective transitions). **Figure 2b** shows the distribution of reversals and recoveries detected over the entire range of forces. This distribution could be fitted by sums of Gaussians. For reversals, we identified one main contribution (16 ± 9 nm), and two minor contributions (35 ± 3 nm and 46 ± 7 nm, mean ± s.d.); for recoveries, we measured a single contribution (12 ± 7 nm). Average amplitudes of all three populations of reversals were independent of load (**Fig. 2c**,**d**). Comparing amplitudes, it is likely that the main reversals are the direct inversions of the recoveries. We attribute the large backward displacements (>25 nm) to slippage along actin (that is, fast detachment and reattachment) because their relative frequency increased with increasing load (**Fig. 2c**,**d**). Slippage along the helical repeat of the actin filament could explain the population of ~35-nm backward displacements, and a combination of slippage and power-stroke reversal could cause displacements with ~46-nm amplitude. This interpretation is supported by the fact that some large backward displacements were followed by a recovery stroke (16 ± 5 nm, **Supplementary Fig. 1f**), although many were followed by detachment.

To be able to directly compare reversals to power strokes in the same experimental conditions, we measured the power stroke produced in the absence of applied load (<2 pN) with a different method. Applying our standard ensemble-averaging technique[21,25], we aligned and averaged myosin binding events using the time points of binding to or detachment from actin, respectively (**Fig. 2e**). As seen before, an initial power stroke (~15 nm) was produced within 1 ms of binding to actin, whereas a much smaller second displacement (~5 nm) followed with a delay of ~29 ms. This is roughly consistent with the reported ADP release rate[4,6,7,26], taking differences in temperature into account (here, k_1 = 24 s^{-1} and T = 29 °C). We carried out these experiments at low ATP (10 μM) so that we could clearly resolve the second displacement and the subsequent, ATP-dependent dwell time (~30 ms)[4,8,21,25]. The ATP binding rate was ~2.4 μM^{-1} s^{-1}, consistent with previous data[6,7,26]. We therefore expected that, in the load experiments that we carried out at 100 μM ATP, the motor would spend most of the actin-bound dwell time in an ADP-bound state because the nucleotide-free rigor state following ADP release would be comparatively short lived (~3 ms for ATP binding and detachment, assuming the above ATP binding rate). Thus, when comparing the reversals at high ATP and high load to the power strokes at low ATP and low load, we need to compare to the initial 15-nm power stroke, not the whole 20-nm power stroke. With these constraints, the numbers support the conclusion that the observed transitions at high load reflect complete reversals and recoveries of the main myosin power-stroke component.

Load-dependent kinetics of power-stroke reversals and recoveries

Next, we evaluated how load affects the kinetics of the observed transitions. Because the transition from pre- to post-state is the main force-generating transition, we expected the dwell times of both the pre- and post-states to be strongly but oppositely affected by load. We therefore analyzed the load dependence of dwell times in the two states (**Fig. 3**, 100 μM ATP). Cumulative distribution plots of dwell times in the pre-state (**Fig. 3a**) were well described by a single exponential function (Online Methods, eq. 1), whereas two exponential components were required to fit the dwell-time distributions in the post-state (**Fig. 3b** and Online Methods, eq. 2). This suggests the existence of two distinct post-states, a short-lived component ($post_1$) and a long-lived component ($post_2$) (**Supplementary Fig. 2**). To keep the scheme (**Fig. 3d**) simple at first, we lumped the two post-states into one and calculated a single rate constant for reversal at different loads (Online Methods, eq. 3). Here we define the reversal rate as the reciprocal of the average dwell time in post-state, whereas the recovery rate is the reciprocal of the dwell time in pre-state (Online Methods). The ratio of the two rates gives the probability to find the motor in either a pre- or a post-state at different loads while bound to actin. The reversal rate increased with increasing load, whereas we observed the opposite for the recovery rate (**Fig. 3c**), consistent with an Arrhenius-type transition between pre- and post-state (eq. 4). An equal probability of finding the motor in pre- or post-state was reached at ~4 pN.

Biochemical state of power-stroke reversals and recoveries

Having collected the evidence for power-stroke reversal still leaves open the question of the degree to which the biochemical pathway is followed backwards (**Fig.4**). Several lines of evidence suggest that acto–myosin-Va has ADP bound at the catalytic site when it is held in a bistable state between pre- and post-state. Given an off-rate

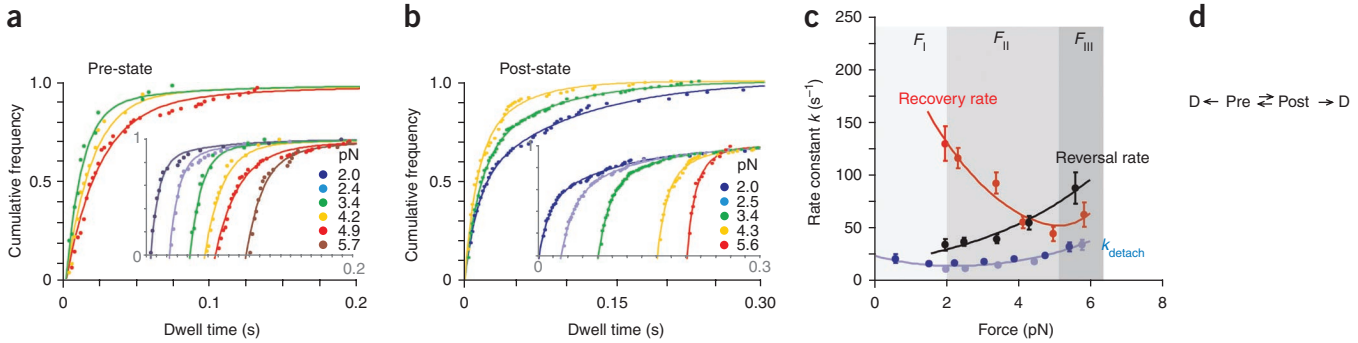

Figure 3 Kinetics of pre- and post-states. (**a**) Cumulative dwell-time distribution plots of the pre-state are described by a single exponential function and yield the recovery rate (eq. 1). (**b**) Two exponential components (eq. 2) were required to describe dwell times of the post-states and yield two reversal rates. Insets, plots at different loads were offset along the time axis for clarity. (**c**) Reversal and recovery rates are plotted against load. The two post-states in **b** (see **Supplementary Fig. 2**) were lumped into one, and a single reversal rate was calculated (eq. 3). Load dependence of recovery rates was described by two exponential components (eq. 5), with $k_{01} = 284\ s^{-1}$, $d_1 = -1.5$ nm and $k_{02} = 0.03\ s^{-1}$, $d_2 = 4.6$ nm. Load dependence of reversals was described by a single exponential (eq. 4) with $k_0 = 17\ s^{-1}$; $d = 1.2$ nm. The detachment rates, k_{detach} = (average time bound)$^{-1}$, are plotted versus load (see **Supplementary Figs. 2** and **3** and **Table 1**); k_{detach} for binding events with and without reversals are plotted in light and dark blue, respectively (see **Supplementary Fig. 4**). Load dependence of the rates was described by two exponential components (eq. 5); $k_{01} = 22\ s^{-1}$, $d_1 = -2.1$ nm and $k_{02} = 3.5\ s^{-1}$; $d_2 = 1.6$ nm. Experiments were carried out at 100 μM ATP. Rate constants and statistics are tabulated in **Supplementary Table 1**. F_I, F_{II} and F_{III} mark three force regimes for which no reversals (F_I), reversals and recoveries (F_{II}) or forced detachments (F_{III}) were observed. (**d**) The model describes transitions between pre- and post-states and detachment (D). The error bars for each data point in **Figure 3c** show the standard error of the mean (SEM).

of > 250 s^{-1} in solution[6], phosphate was probably mostly released by the time load was applied (after ~3 ms). The concentration of phosphate in solution was low (<2 μM) and made phosphate rebinding unlikely. To investigate whether phosphate could rebind to the acto–MVS1 complex under load, we did a control experiment (**Fig. 4b**) which shows that, at forces >2 pN, the addition of 10 mM phosphate increases the rate constant for unbinding by a factor of 2. This suggests that phosphate may rebind and that the phosphate-bound pre-state (A.M.ADP.Pi) detaches more easily. This is consistent with previous reports that this state is bound more weakly[27,28]. The effect of phosphate could also be nonspecific, but this appears unlikely because we did not observe the effect in the absence of load (**Fig. 4b**). This is consistent with a partial reversal of the chemical cycle coupled to the reversal of the mechanical cycle. It further follows that most motors must have had their phosphate released before load was applied in our experiments when phosphate was not added. Finally, it was also unlikely that the motor dwelled in a nucleotide-free rigor state as argued above because we intentionally worked at high ATP concentration (100 μM). Thus, all the evidence suggests that the myosin motor in the 'rocking crossbridge' state has released phosphate and retains ADP.

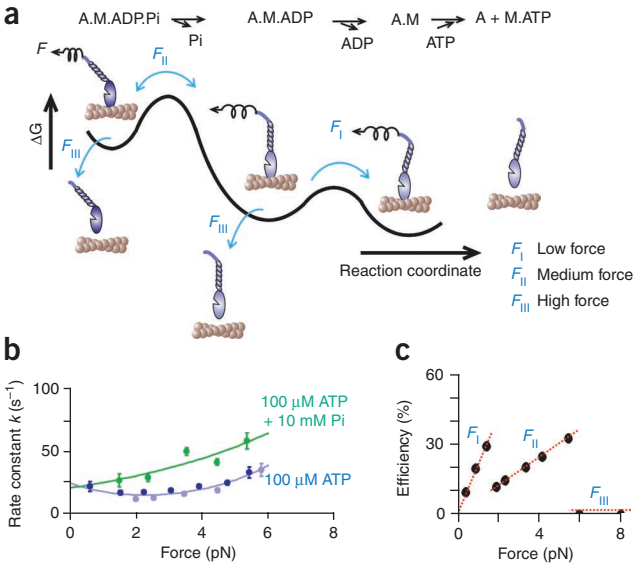

Figure 4 Effect of load on a single MVS1 motor head. (**a**) The model summarizes the effect of low (F_I), medium (F_{II}) and high loads (F_{III}) on the chemomechanical cycle of a single MVS1 motor head. (**b**) Rate constants characterizing the average dwell time of MVS1 bound to actin in the absence and presence of 10 mM phosphate are plotted versus load. Load dependence in the presence of 10 mM phosphate was described by a single exponential function (eq. 4), with $k_0 = 24\ s^{-1}$ and $d = 0.6$ nm (see also **Supplementary Fig. 4c**). For comparison, load dependence of dwell times in the absence of added phosphate is plotted in blue (data from **Fig. 3c**). (**c**) Efficiency of energy conversion of a single motor head in the three load regimes (F_I–F_{III}).

DISCUSSION

In summary, our experiments have provided a new view on the mechanochemical energy landscape guiding myosin force generation (**Fig. 4a**). Two lines of evidence suggest that, at high loads, the MVS1 motor can switch back and forth between post- and pre-state while remaining bound to actin. First, the amplitudes of reversals and recoveries were similar, independent of load and matched the main component[11,29,30] of the two-step power stroke[4,8,21] at low load. Second, the dwell times of reversals became longer at increasing load, whereas those of recoveries became shorter, as expected. This finding is direct evidence for the 'rocking crossbridge', which was hypothesized[31] but never observed at the level of a single molecule.

The effect of load on a single MVS1 motor head can be divided into three force regimes (**Figs. 3c** and **4a**). At low forces F_I (0–2 pN), the actin-bound dwell time increased with load. At intermediate forces F_{II} (2–5 pN), the motor switched back and forth between pre- and post-state. At high forces F_{III} (5–7 pN), the motor dwelled predominantly in the pre-state before being forced to detach.

At low forces F_I, actin-bound dwell times increased about two-fold with load. This is consistent with a load-dependent and rate-limiting ADP release[2,4,6,7,18,21,30,32]. ATP binding, in contrast, was shown to be weakly load dependent[21,30,33], and the rigor state is negligible at high ATP (100 μM) as discussed. ADP release is probably slowed down

because the second step of the working stroke, associated with ADP release, is hindered[8,21]. The sensitivity of a biochemical transition to load is typically expressed as a distance d to the transition state[34]. We find here that d = 2.1 nm (at 29 °C, **Fig. 3c**), which is roughly consistent with, though slightly smaller than, what we found previously (d = 4.3 nm at 23 °C, ref. 21). This difference might be due to differences in temperature[26]. Previous work[16] reported an even larger distance of 12.5 nm for ADP release. However, these results can perhaps be reconciled. A strong sensitivity to force is exactly what one expects approaching a nonlinearity in response, such as power-stroke reversal. In previous work[16], an increased sensitivity to load was observed in the range of 1.5–2 pN, which is precisely where we begin to see power-stroke reversals. Also, at this force, processive backward stepping of the dimeric motor has been observed[27,35].

Although backward load only weakly affects total duration of myosin binding at intermediate force F_{II} (2–5 pN), it shifts the motor increasingly into a pre–power stroke ADP-bound state. Our 'stall force' (~4 pN) for a single head (that is, the force that results in an equal probability to dwell in pre– and post–power stroke conformation) is somewhat higher than the external force required to stall processive movement of the myosin-Va dimer (1.7–3 pN)[2,4,16,18,19,27]. The difference is likely due to differences in the geometry of force application. For the full-length dimer, the effective lever arm is likely to be longer than in our single-headed construct, which can qualitatively explain the difference.

What is the relevance of the power-stroke reversibility for the mechanical head-head communication during processive forward movement of a myosin-Va dimer? Because of differences in geometry, it is again difficult to directly compare absolute forces. However, it is conceivable that the force exerted by the trailing head on the leading head is enough to keep the leading head in the pre-state until the trailing head detaches, as suggested by electron and fluorescence microscopy[10–12,36] and solution kinetic studies[3,7,37,38] (**Supplementary Fig. 5**, i and ii). This scenario is also consistent with our previous observation[4,21] of an only twofold acceleration of ADP release on the trailing head in the dimer compared to that of a single head. The twofold acceleration would correspond to a force of ~1.5–2 pN[4,21,39], less than what would be expected if the leading head was in post-state (~3.5 pN)[21,39].

We also found rare binding events with very slow detachment kinetics in this force range F_{II} (**Supplementary Table 1**), similar to what was described for processive backward stepping of myosin-Va at super-stall forces[19]. As only the reversals (post-state) but not the recoveries (pre-state) show a slow component, the motor spending time in post$_2$ must be responsible for the slow kinetics (**Supplementary Fig. 2**). At present, the exact nature of the post$_1$ and post$_2$ states is not clear. During processive forward movement at low load, both ADP-bound states might occur in sequence (**Fig. 4a**, A.M.ADP, and **Supplementary Fig. 2a**), with the shorter-lived post$_1$ first followed by an isomerization to the more stable post$_2$ (refs. 7,38,40).

At high forces F_{III} (5–7 pN), we found that the motor was forced to detach, predominantly from the pre-state. This is consistent with previously measured unbinding forces for a single myosin-Va head[32,41].

If we want to determine the efficiency of a single motor head at increasing load, we simply need to know whether the head detaches from pre- or post-state. Efficiency can be defined as the total work done against external load up to a time point immediately before detachment, divided by the free energy gained by hydrolysis of one ATP molecule. In regime F_I (<2 pN, **Fig. 4c**), we did not observe reversals, and therefore, the motor always detached from the post-state. The efficiency E is $E = Fd_{stroke} / \Delta G_{ATP}$. In regime F_{II} (2–5 pN), the motor detaches in approximately 30% of binding events from the post-state (**Supplementary Fig. 1e**). Here $E = F0.3d_{stroke} / \Delta G_{ATP}$, whereas in force regime F_{III}, the motor detaches predominantly from the pre-state and does not produce work. What does this signify for the efficiency of the dimer? Maximum work output can be expected at near-stall force, but the precise value of the efficiency will depend on the exact geometries of forces and motion.

Complex load sensitivity at different stages of the chemomechanical cycle, as observed here, has obvious implications for the collective dynamics of myosin motors. Load-dependent ADP release might contribute to coordinating the two heads of processive dimeric myosin-Va[3,4,7,19,21,32]. Reversibility of the power stroke at higher loads provides, on the one hand, a microscopic mechanism for backward sliding at super-stall forces[19]. On the other hand, reversibility of the power stroke is equivalent to a highly nonlinear response, which can lead to mechanical synchronizations and oscillations. Power-stroke reversals could thus be involved in the wide range of such phenomena—for example, in certain types of muscle[42,43] or in mechanoreceptive hair bundles in the sensory cells of the inner ear[44,45].

METHODS

Methods and any associated references are available in the online version of the paper at http://www.nature.com/nsmb/.

Note: Supplementary information is available on the Nature Structural & Molecular Biology website.

ACKNOWLEDGMENTS

We thank C. Schmidt and J. Molloy for stimulating discussions, E. Harvey for technical assistance and J. Hammer III (Laboratories of Cell Biology, National Heart, Lung, and Blood Institute, US National Institutes of Health) for kindly supplying the myosin-Va clone. We are also grateful to the UK Medical Research Council, The Royal Society UK and the US National Institutes of Health for grant support.

AUTHOR CONTRIBUTIONS

J.R.S. expressed and purified MVS1; C.V. carried out experiments and data analysis; J.R.S. and C.V. wrote the paper.

COMPETING FINANCIAL INTERESTS

The authors declare no competing financial interests.

Published online at http://www.nature.com/nsmb/.
Reprints and permissions information is available online at http://npg.nature.com/reprintsandpermissions/.

1. Sellers, J.R. & Veigel, C. Walking with myosin V. *Curr. Opin. Cell Biol.* **18**, 68–73 (2006).
2. Mehta, A.D. *et al.* Myosin-V is a processive actin-based motor. *Nature* **400**, 590–593 (1999).
3. Sakamoto, T., Webb, M.R., Forgacs, E., White, H.D. & Sellers, J.R. Direct observation of the mechanochemical coupling in myosin Va during processive movement. *Nature* **455**, 128–132 (2008).
4. Veigel, C., Wang, F., Bartoo, M.L., Sellers, J.R. & Molloy, J.E. The gated gait of the processive molecular motor, myosin V. *Nat. Cell Biol.* **4**, 59–65 (2002).
5. Yildiz, A. *et al.* Myosin V walks hand-over-hand: Single fluorophore imaging with 1.5-nm localization. *Science* **300**, 2061–2065 (2003).
6. De La Cruz, E.M., Wells, A.L., Rosenfeld, S.S., Ostap, E.M. & Sweeney, H.L. The kinetic mechanism of myosin V. *Proc. Natl. Acad. Sci. USA* **96**, 13726–13731 (1999).
7. Rosenfeld, S.S. & Sweeney, H.L. A model of myosin V processivity. *J. Biol. Chem.* **279**, 40100–40111 (2004).
8. Volkmann, N. *et al.* The structural basis of myosin V processive movement as revealed by electron cryomicroscopy. *Mol. Cell* **19**, 595–605 (2005).
9. Coureux, P.D., Sweeney, H.L. & Houdusse, A. Three myosin V structures delineate essential features of chemo-mechanical transduction. *EMBO J.* **23**, 4527–4537 (2004).
10. Walker, M.L. *et al.* Two-headed binding of a processive myosin to F-actin. *Nature* **405**, 804 (2000).
11. Burgess, S. *et al.* The prepower stroke conformation of myosin V. *J. Cell Biol.* **159**, 983–991 (2002).

12. Forkey, J.N., Quinlan, M.E., Shaw, M.A., Corrie, J.E.T. & Goldman, Y.E. Three-dimensional structural dynamics of myosin V by single-molecule fluorescence polarization. *Nature* **422**, 399–404 (2003).
13. Toprak, E. *et al.* Defocused orientation and position imaging (DOPI) of myosin V. *Proc. Natl. Acad. Sci. USA* **103**, 6495–6499 (2006).
14. Dunn, A.R. & Spudich, J.A. Dynamics of the unbound head during myosin V processive translocation. *Nat. Struct. Mol. Biol.* **14**, 246–248 (2007).
15. Cappello, G. *et al.* Myosin V stepping mechanism. *Proc. Natl. Acad. Sci. USA* **104**, 15328–15333 (2007).
16. Uemura, S., Higuchi, H., Olivares, A.O., De La Cruz, E.M. & Ishiwata, S. Mechanochemical coupling of two substeps in a single myosin V motor. *Nat. Struct. Mol. Biol.* **11**, 877–883 (2004).
17. Shiroguchi, K. & Kinosita, K. Myosin V walks by lever action and Brownian motion. *Science* **316**, 1208–1212 (2007).
18. Rief, M. *et al.* Myosin-V stepping kinetics: a molecular model for processivity. *Proc. Natl. Acad. Sci. USA* **97**, 9482–9486 (2000).
19. Gebhardt, J.C.M., Clemen, A.E.M., Jaud, J. & Rief, M. Myosin-V is a mechanical ratchet. *Proc. Natl. Acad. Sci. USA* **103**, 8680–8685 (2006).
20. Carter, N.J. & Cross, R.A. Mechanics of the kinesin step. *Nature* **435**, 308–312 (2005).
21. Veigel, C., Schmitz, S., Wang, F. & Sellers, J.R. Load-dependent kinetics of myosin-V can explain its high processivity. *Nat. Cell Biol.* **7**, 861–869 (2005).
22. Finer, J.T., Simmons, R.M. & Spudich, J.A. Single myosin molecle mechanics-piconewton forces and nanometre steps. *Nature* **368**, 113–119 (1994).
23. Veigel, C., Bartoo, M.L., White, D.C.S., Sparrow, J.C. & Molloy, J.E. The stiffness of rabbit skeletal actomyosin cross-bridges determined with an optical tweezers transducer. *Biophys. J.* **75**, 1424–1438 (1998).
24. Molloy, J.E., Burns, J.E., Kendrick-Jones, J., Tregear, R.T. & White, D.C.S. Movement and force produced by a single myosin head. *Nature* **378**, 209–212 (1995).
25. Veigel, C. *et al.* The motor protein myosin-I produces its working stroke in two steps. *Nature* **398**, 530–533 (1999).
26. Robblee, J.P., Cao, W.X., Henn, A., Hannemann, D.E. & De La Cruz, E.M. Thermodynamics of nucleotide binding to actomyosin V and VI: a positive heat capacity change accompanies strong ADP binding. *Biochemistry* **44**, 10238–10249 (2005).
27. Kad, N.M., Trybus, K.M. & Warshaw, D.M. Load and Pi control flux through the branched kinetic cycle of myosin V. *J. Biol. Chem.* **283**, 17477–17484 (2008).
28. Takagi, Y., Shuman, H. & Goldman, Y.E. Coupling between phosphate release and force generation in muscle actomyosin. *Phil. Trans. R. Soc. Lond. B* **359**, 1913–1920 (2004).
29. Moore, J.R., Krementsova, E.B., Trybus, K.M. & Warshaw, D.M. Myosin V exhibits a high duty cycle and large unitary displacement. *J. Cell Biol.* **155**, 625–635 (2001).
30. Purcell, T.J., Sweeney, H.L. & Spudich, J.A. A force-dependent state controls the coordination of processive myosin V. *Proc. Natl. Acad. Sci. USA* **102**, 13873–13878 (2005).
31. Huxley, A.F. & Simmons, R.M. Proposed mechanism of force generation in striated muscle. *Nature* **233**, 533–538 (1971).
32. Oguchi, Y. *et al.* Load-dependent ADP binding to myosins V and VI: implications for subunit coordination and function. *Proc. Natl. Acad. Sci. USA* **105**, 7714–7719 (2008).
33. Veigel, C., Molloy, J.E., Schmitz, S. & Kendrick-Jones, J. Load-dependent kinetics of force production by smooth muscle myosin measured with optical tweezers. *Nat. Cell Biol.* **5**, 980–986 (2003).
34. Howard, J. *Mechanics of Motor Proteins and the Cytoskeleton* 76–89 (Sinauer, Sunderland, Massachusetts, USA, 2001).
35. Clemen, A.E.M. *et al.* Force-dependent stepping kinetics of myosin-V. *Biophys. J.* **88**, 4402–4410 (2005).
36. Syed, S., Snyder, G.E., Franzini-Armstrong, C., Selvin, P.R. & Goldman, Y.E. Adaptability of myosin V studied by simultaneous detection of position and orientation. *EMBO J.* **25**, 1795–1803 (2006).
37. Forgacs, E. *et al.* Kinetics of ADP dissociation from the trail and lead heads of actomyosin V following the power stroke. *J. Biol. Chem.* **283**, 766–773 (2008).
38. Hannemann, D.E., Cao, W.X., Olivares, A.O., Robblee, J.P. & De La Cruz, E.M. Magnesium, ADP, and actin binding linkage of myosin V: evidence for multiple myosin V-ADP and actomyosin V-ADP states. *Biochemistry* **44**, 8826–8840 (2005).
39. Vilfan, A. Elastic lever-arm model for myosin V. *Biophys. J.* **88**, 3792–3805 (2005).
40. Nyitrai, M.G.M.A. Adenosine diphosphate and strain sensitivity in myosin motors. *Phil. Trans. R. Soc. Lond. B* **359**, 1867–1877 (2004).
41. Nishizaka, T., Miyata, H., Yoshikawa, H., Ishiwata, S. & Kinosita, K. Unbinding force of a single motor molecule of muscle measured using optical tweezers. *Nature* **377**, 251–254 (1995).
42. Duke, T.A.J. Molecular model of muscle contraction. *Proc. Natl. Acad. Sci. USA* **96**, 2770–2775 (1999).
43. Shimamoto, Y., Suzuki, M. & Ishiwata, S. Length-dependent activation and auto-oscillation in skeletal myofibrils at partial activation by Ca^{2+}. *Biochem. Biophys. Res. Commun.* **366**, 233–238 (2008).
44. Hudspeth, A.J. & Gillespie, P.G. Pulling springs to tune transduction—adaptation by hair-cells. *Neuron* **12**, 1–9 (1994).
45. Kruse, K. & Julicher, F. Oscillations in cell biology. *Curr. Opin. Cell Biol.* **17**, 20–26 (2005).

ONLINE METHODS

Protein preparations, solutions and optical trapping conditions. We used a baculovirus-expressed MVS1 as described previously[21]. Details of the myosin construct, biochemical solutions and optical trapping conditions are described in **Supplementary Information**. Procedures to apply load and details on data analysis are given below and also in **Supplementary Information**.

Application of load. To improve time resolution for detecting myosin binding, we oscillated the position of one optical trap at a frequency $f = 1$ kHz and amplitude $A_0 = 35$ nm parallel to the actin filament axis using a sinusoidal function[25,33]. Because of low trap stiffness and viscous damping, the position of the bead-actin-bead dumbbell held in the traps oscillated parallel to the filament axis, with r.m.s. amplitude of only ~7 nm during the intervals when no myosin was bound to actin. During periods when myosin was bound, this r.m.s. amplitude was further reduced to less than 1.5 nm, so that the mechanical disturbance of the bound myosin was very small (corner frequency of thermal noise during attachment ~3 kHz; r.m.s. of 1-kHz signal close to thermal background noise). By analyzing changes in variance of the high-pass filtered displacement signal (dominated by the 1-kHz signal during periods when myosin was not bound) transmitted to the bead in the other (passive) trap, we could detect myosin binding with ~1-ms time resolution[21]. Changes in this signal were used to produce a trigger signal. The latter was used to change the position of both optical traps[33]. To apply load, both traps were moved by a distance dx_{trap} in parallel to the actin filament axis to produce a force, $F = 2\kappa_{trap}\Delta x$ (κ_{trap}, single trap stiffness; $\Delta x = x_{trap} - x_{bead}$; x_{trap}, trap position; x_{bead}, bead position)[23]. Here we assume the stiffness of both traps to be the same. Following detection of myosin detachment, the traps were returned to their rest position, again with a time delay of ~3 ms. Initial binding and conformational change occurred within less than our time resolution, so that the direction of the initial conformational change was not resolved in individual binding events. We therefore determined the direction of the conformational change (power stroke) for each actin dumbbell by analyzing an ensemble of myosin binding events in absence of load[24] before load experiments were performed.

Analysis of amplitudes of reversals and recoveries. Data analysis was carried out on the displacement data recorded from the bead held in the passive trap. Amplitudes and dwell times of reversals and recoveries were analyzed off line in an automated fashion. The *t*-test values were calculated from the time series of variance and mean displacement over a running time window of 20 data points. To determine the amplitudes of reversals and recoveries, we calculated the time-averaged displacement between level changes. Amplitudes were calculated relative to the preceding level.

When load was applied by moving both traps in a stepwise fashion, the actin dumbbell, connected to the surface via myosin, first produced a passive, series elastic response (**Supplementary Fig. 1a**). To separate the elastic response from subsequent power-stroke reversals, we determined the bead position 2 ms after load was applied and the system had relaxed[46]. This bead position was used as reference for subsequent reversals.

Analysis of dwell times. The minimum dwell time t_{min} of a myosin binding event, we evaluated, was $t_{min} = 10$ ms. t_{min} of pre- and post-states evaluated during a binding event was $t_{min} = 4$ ms, and the maximum dwell time was $t_{max} = 500$ ms. Dwell-time distributions of pre- and post-states were plotted as cumulative and normalized distributions. Rate constants *k* were obtained by least-squares fitting of the model functions. **Figure 3d** shows the reaction scheme used to describe transitions between pre- and post-state and detachment. Cumulative dwell-time distributions were described by a probability-density function, taking the limits t_{min} and t_{max} into account[19,47]. If a single exponential could be used to describe the distribution, the function was:

$$P_b(t) = \frac{\exp(-kt) - \exp(-kt_{min})}{\exp(-kt_{max}) - \exp(-kt_{min})} \quad (1)$$

The exit rate out of a state k is equal to the reciprocal of the average dwell time of that state.

If two exponential components were required to fit the dwell time distributions, the probability density function was:

$$P_b(t) = \frac{Z_1(\exp(-k_1 t) - \exp(k_1 t_{min})) + (1 - Z_1)(\exp(-k_2 t) - \exp(-k_2 t_{min}))}{Z_1(\exp(-k_1 t_{max}) - \exp(k_1 t_{min})) + (1 - Z_1)(\exp(-k_2 t_{max}) - \exp(-k_2 t_{min}))} \quad (2)$$

Z_1 and $(1 - Z_1)$ are the relative amplitudes of the fast and slow component, respectively.

If binding events ended on a reversal, these last reversals preceding detachment were not taken into account in the kinetic analysis because they could be due to reversal of the power stroke or slippage along actin. If slippage had occurred, the state would be ambiguous; that is, it could be either the pre- or post-state (see **Supplementary Discussion**). The exit rate *k* out of the pre-state in our analysis thus characterizes the transition into post-state and is called recovery rate.

The state before the first reversal in a binding event has to be a post-state. Therefore, we included these dwell times into the population of post-states. At all loads, most of the binding events ended on a backward displacement (**Supplementary Fig. 1e**). The exit rate *k* out of the post-state in our analysis therefore mostly characterizes transition into pre-state and is called reversal rate.

The average reversal rate *k* at different loads was calculated from the two reversal rates k_1 and k_2 obtained from the dwell-time distibutions of the post-state (**Fig. 3b**):

$$k = 0.5(Z_1 k_1 + (1 - Z_1)k_2) \quad (3)$$

Load dependence of the average and the two individual reversal rates k_1 and k_2 was described by an Arrhenius-type transition over an activation energy barrier:

$$k(F) = k_0 \exp(-\frac{Fd}{k_b T}) \quad (4)$$

$k(F)$, load-dependent rate; k_0, rate in absence of load; F, force; d, distance parameter; $k_b T$, thermal energy.

For the recovery rate and for the detachment rate of motors, two exponential components were required to describe their load dependence:

$$k(F) = k_{01} \exp(-\frac{Fd_1}{k_b T}) + k_{02} \exp(-\frac{Fd_2}{k_b T}) \quad (5)$$

Preparation of figures. Figures were generated using standard software.

46. van Mameren, J., Vermeulen, K.C., Gittes, F. & Schmidt, C.F. Leveraging single protein polymers to measure flexural rigidity. *J. Phys. Chem. B* **113**, 3837–3844 (2009).
47. Colquhoun, D. & Sigworth, F.J. Practical analysis of records. in. *Single Channel Recording* (eds. Sakmann, B. & Neher, E.) 558–563 (Plenum Press, New York, USA, 1995).

doi:10.1038/nsmb.1820